

# Securing Satellite Communications: Real-Time Video Encryption Scheme on Satellite Payloads

Hanshuo Qiu, Jing Lian, Xiaoyuan Wang, and Jizhao Liu\*

**Abstract**—The rapid development of low-Earth orbit (LEO) satellite constellations and satellite communication systems has elevated the importance of secure video transmission, which is the key to applications such as remote sensing, disaster relief, and secure information exchange. In this context, three serious issues arise concerning real-time encryption of videos on satellite embedded devices: (a) the challenge of achieving real-time performance; (b) the limitations posed by the constrained computing performance of satellite payloads; and (c) the potential for excessive power consumption leading to overheating, thereby escalating safety risks. To overcome these challenges, this study introduced a novel approach for encrypting videos by employing two 1D chaotic maps, which was deployed on a satellite for the first time. The experiment on the satellite confirms that our scheme is suitable for complex satellite environments. In addition, the proposed chaotic maps were implemented on a Field Programmable Gate Array (FPGA) platform, and simulation results showed consistency with those obtained on a Raspberry Pi. Experiments on the Raspberry Pi 4B demonstrate exceptional real-time performance and low power consumption, validating both the hardware feasibility and the stability of our design. Rigorous statistical testing also confirms the scheme’s resilience against a variety of attacks, underscoring its potential for secure, real-time data transmission in satellite communication systems.

**Index Terms**—chaos, chaotic encryption, satellite communication, multimedia communication

## I. INTRODUCTION

With the rapid advancement of satellite communication and the deployment of low-Earth orbit (LEO) satellite constellations, video data has become a critical information carrier in satellite communication systems, supporting applications such as remote sensing, disaster relief, and secure information exchange [1]. However, the transmission of video data in satellite communication faces increasingly serious security threats, including information leakage, theft, and data distortion [2]. These security risks may not only endanger the functionality of the device and user privacy but also pose potential risks to national security. Consequently, the development of efficient and reliable encryption technology has become a core requirement for ensuring data security and privacy in satellite communications [3].

Existing video encryption algorithms can be broadly classified into two categories: traditional methods (e.g., DES, AES, and RSA) and chaos-based techniques [4]. Due to the complex

mechanisms and the inherent redundancy in multimedia data, the effectiveness of traditional encryption in real-time satellite communication is hindered by limited encryption speed, particularly within the resource-constrained environments, such as portable satellite devices and LEO systems [5]. Furthermore, conventional encryption methods often fail to preserve video storage formats, complicating real-time processing and playback [6]. The application of chaotic maps in cryptosystems has grown due to their sensitivity to initial conditions, randomness, and unpredictability, making them suitable for secure and adaptive video encryption in dynamic satellite communication environments [7]–[9]. Due to these characteristics and the fast growth in both the practical implementation and theoretical understanding of chaos, a growing number of researchers have turned their attention towards the development of chaotic cryptography methods [10], [11]. These developments underscore the potential of chaos-based approaches as a compelling alternative for addressing the unique security and performance challenges in satellite video transmission.

In the context of satellite communication applications, the demand for secure video transmission on satellites is escalating, leading to a more widespread trend towards the adoption of video encryption. However, the deployment of encryption schemes on satellite payloads entails corresponding challenges: (a) Due to the complexity of encryption schemes, most video stream encryption approaches face challenges in achieving real-time characteristics. (b) The deployment of complex, high-performance equipment is hampered by the instability stemming from harsh environments. In comparison to ground-based high-performance computing devices, satellite devices generally possess fewer computing resources, thereby exacerbating challenges to the efficiency and stability of video encryption. (c) Due to the challenges of heat dissipation in a vacuum environment, the power required to operate the encryption algorithm must be confined within a specific range. Excessive power consumption may lead to overheating, resulting in equipment damage. However, overly high encryption speeds can also result in increased power consumption. Therefore, it is crucial to strike a balance between power consumption and encryption speed to ensure both system stability and performance. These challenges are shown in Fig. 1.

In this study, we proposed a novel video encryption algorithm based on 1D chaotic mapping and deployed it in a satellite environment for the first time. To overcome the three difficulties shown in Fig. 1, four key strategies are employed: (a) Utilization of novel 1D chaotic systems. We integrate the 1D chaotic map, which is known for its simplicity and rapidity, into our encryption scheme to significantly boost real-time

H. Qiu and J. Liu are with the School of Information Science and Engineering, Lanzhou University, No.222, TianShui Road(south), Lanzhou, 730000, Gansu, China.

J. Lian is with the School of Electronics and Information Engineering, Lanzhou Jiaotong University, Lanzhou, 730070, Gansu, China.

X. Wang is with the School of Electronics and Information, Hangzhou Dianzi University, Hangzhou 310018, China.

\*Corresponding author: Jizhao Liu (email: liujz@lzu.edu.cn).

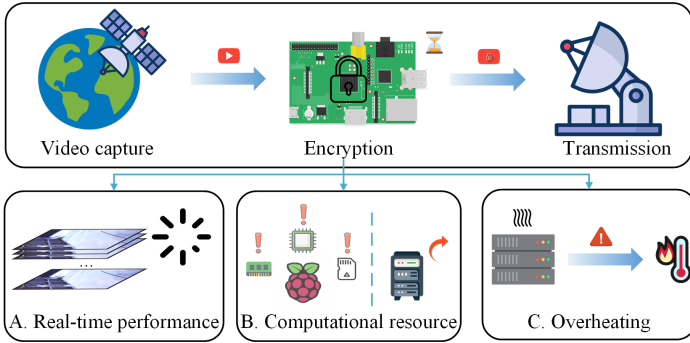


Fig. 1. Satellite video communication framework and challenges of real-time video encryption on satellite payloads.

performance. (b) Implementation of the algorithm using C++. C++ is selected for its high performance and ability to handle computationally intensive operations with minimal latency. These characteristics make it ideal for real-time applications in resource-constrained satellite communication systems. (c) Simplification of the encryption process to a single XOR operation, which diminishes both computational complexity and encryption duration. The `bitwise_xor` function in the OpenCV library further optimizes the encryption process by providing a highly efficient and hardware-accelerated operation for handling binary data, ensuring both speed and compatibility with embedded platforms. (d) Preservation of the final encrypted data in binary format. Binary storage substantially reduces the time necessitated for data storage and guarantees its intact retention without any loss. The proposed chaotic mapping was employed on a Field Programmable Gate Array (FPGA) platform, and simulation results showed consistent performance with those obtained on the Raspberry Pi platform, confirming its feasibility and stability across different satellite edge devices. Comprehensive statistical tests (NIST and DIEHARD) and various attack simulations further validate the robustness and security of our encryption system. Additionally, our timing analysis and power consumption analysis, which are conducted on the Raspberry Pi 4B, confirm the feasibility of real-time encryption of high-definition videos on a satellite payload, making it a promising solution for secure, real-time data transmission in satellite communication systems.

The main contributions of this work are as follows:

- 1) We designed two novel and efficient 1D chaotic maps that are more effective in meeting real-time requirements in resource-constrained satellite communication systems compared to other chaotic maps. The lightweight bit shift operations in chaotic maps instead of floating-point arithmetic enhance the overall efficiency of the system. Additionally, due to their low-dimensional characters, we fully utilize the computation results from each iteration, maximizing efficiency and reducing redundancy in the process. The visual analysis and Poincare maps from the experiments confirm the complex chaotic behavior. Furthermore, this chaotic map successfully passed the DIEHARD test suite, demonstrating its high level of unpredictability.

- 2) We introduced a novel video encryption scheme employing 1D chaotic mapping, including four important strategies: the adoption of novel 1D chaotic mapping, implementation using C++, the reduction of the encryption process to a single `bitwise_xor` operation, and its storage in a binary file format. In addition, we considered two different application scenarios for satellite communication systems: (a) The first scenario involves the complete encryption process, including read, encrypt, and write operations, which is designed for applications that require end-to-end security. This application scenario is suited for the encryption of up to 1K resolution videos. (b) The second scenario focuses only on the encryption algorithm, analyzing whether the algorithm is suitable for real-time applications that are integrated into existing workflows. This application scenario can support video encryption for resolutions up to 2K.
- 3) To the best of our knowledge, we first deployed a real-time video encryption algorithm on the satellite. The files and data transmitted from the satellite confirm that our algorithm can adapt to the complex space environment. This scheme successfully passed various image encryption tests, showcasing excellent real-time performance, low energy consumption, and compatibility with satellite embedded devices.

The rest of this paper is organized as follows: Section II introduces the related work. We then propose the encryption scheme in Section III. In Section IV, we discuss the performance and security analysis. Finally, the conclusions are drawn in Section V.

## II. RELATED WORK

### A. Existing Chaos-Based Encryption Algorithms

Chaotic maps may be categorized into two types: one-dimensional (1D) and high-dimensional chaotic maps. High-dimensional maps offer stronger security but are complex and time-consuming, making them inappropriate for real-time video encryption on satellite communication systems. In contrast, 1D chaotic maps, because of their uncomplicated structure, may be readily implemented, which is a very desirable characteristic in cryptography. Therefore, given the constraints of satellite communication systems, such as limited computational resources and the need for real-time processing, it is more appropriate to utilize 1D chaotic mapping for real-time video encryption.

Yang et al. presented a 2D map employed in the design of an S-box for image encryption, indicating high performance and robustness against various attacks [12]. Singh et al. proposed a novel encryption scheme based on chaotic systems and the DNA algorithm [13]. Zhao et al. proposed a novel satellite image encryption algorithm that combines RNA computations with seven-dimensional complex chaotic systems, increasing security through scrambling and diffusion phases [14].

### B. Video Encryption Schemes

Previous research has introduced a variety of encryption methodologies. Li et al. developed a novel encryption algorithm adapted to the H.264 standard [15]. Duan et al.

introduced a CNN-based video encryption technique utilizing Faster RCNN [16]. Fadi et al. encrypted the video information through the RTP protocol [17].

While these solutions offer high security due to numerous iterations and extensive calculations, they lack optimal efficiency and struggle to facilitate real-time encryption. Furthermore, the majority of experiments are conducted on computing devices equipped with high-performance processors, neglecting the consideration of limited computing resources in satellite communication systems. Particularly for performance-constrained satellite embedded systems, these encryption schemes present significant challenges to achieving real-time encryption.

### III. PROPOSED METHOD

#### A. Problem Statement and Challenges

Achieving real-time video encryption is crucial for satellite communications. However, existing encryption algorithms struggle to deliver optimal real-time performance due to their substantial computational complexity, as depicted in Fig. 1A. Furthermore, the harsh satellite environment and unstable energy supply hamper the deployment of high-performance satellite equipment, complicating the assurance of real-time performance and reliability for satellite communication systems. Additionally, the unique space environment makes heat dissipation a significant challenge, necessitating strict power range control for programs operating in satellite conditions and achieve a balance between power consumption and encryption speed. Thus, exploring real-time video encryption solutions that are suitable for satellite payloads becomes imperative to support the secure and resilient operation of satellite communication systems.

#### B. Novel 1D Chaotic Map

In order to tackle the difficulties mentioned in Section III-A, this study employs a discrete-space chaotic map to avoid the expensive integer division procedure. Ref. [18] uses discrete-space chaos mapping to avoid floating-point techniques, resulting in improved memory access efficiency. The formula is shown in Eq. (1). While the initial chaotic map has low computational complexity and is appropriate for real-time video encryption, we have made modifications to transform the 2D discrete-space chaotic map into two novel 1D chaotic maps. This alteration aims to further decrease the time required for generating pseudo-random sequences while ensuring the efficient utilization of the generated sequences. The two novel chaotic maps are shown in Eq. (2) and Eq. (3), respectively.

$$\begin{cases} a = (w \ll (w \% 64)) \mid (w \gg (64 - w \% 64)) \\ w = \left(\frac{a}{2^{32}} + 1\right) \times (a \% 2^{32} + 1) + 1 \end{cases} \quad (1)$$

$$y_k = \begin{cases} (y_{k-1} \ll (y_{k-1} \% 64)) \mid \\ (y_{k-1} \gg (64 - y_{k-1} \% 64)) & \text{if } k \% 2 = 1 \\ \left(\frac{y_{k-1}}{2^{32}} + 1\right) \times \\ (y_{k-1} \% 2^{32} + 1) + 1 & \text{if } k \% 2 = 0 \end{cases} \quad (2)$$

$$y_k = \begin{cases} (y_{k-1} \ll (y_{k-1} \% 64)) \mid \\ (y_{k-1} \gg (64 - y_{k-1} \% 64)) & \text{if } k \% 2 = 0 \\ \left(\frac{y_{k-1}}{2^{32}} + 1\right) \times \\ (y_{k-1} \% 2^{32} + 1) + 1 & \text{if } k \% 2 = 1 \end{cases} \quad (3)$$

The Poincare map is the point where a periodic orbit of a continuous dynamical system intersects a lower-dimensional subspace called the Poincare section, which is positioned in a way that it cuts across the flow of the system [19]. Chaotic motion occurs when the Poincare section shows continuous curves or a large number of densely packed points [20]. Fig. 2 provides evidence of the system's chaotic behavior.

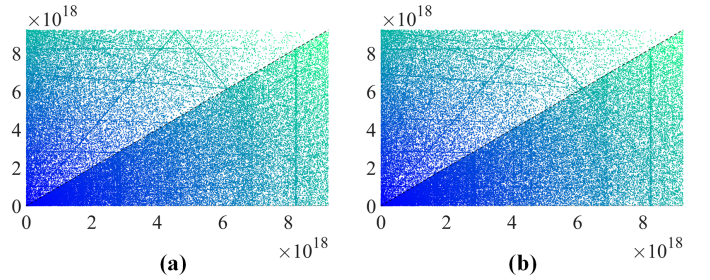


Fig. 2. Poincare section of the novel 1D chaotic map: (a) chaotic map (2), (b) chaotic map (3).

To assess the level of unpredictability in the pseudo-random sequence, the same initial values were applied to two chaotic maps, and the first 400 items were retrieved from each map. Fig. 3 illustrates each value within the first 400 elements of the two chaotic maps. It is shown that the difference between consecutive elements indicates exceptional randomness. Furthermore, the two sequences are entirely distinct, reflecting the inherent differences between the chaotic maps.

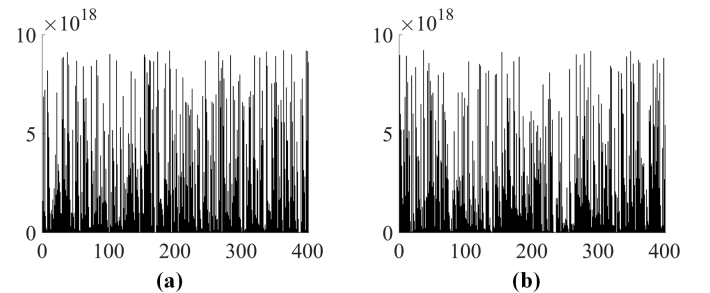


Fig. 3. Visual representation of novel 1D chaotic map: (a) chaotic map (2), (b) chaotic map (3).

The DIEHARD test suite consists of 17 distinct tests used to validate the randomness of a given sequence [21]. A sequence is considered to have passed the test at a significance level of 0.05 if the resulting  $P$  values lie within the range of  $0.025 < P < 0.975$ . Tab. I demonstrates the pronounced randomness of two chaotic sequences. (✓) is used to indicate that the test was successfully passed.

TABLE I  
RESULT OF DIEHARD TESTS SUITE.

Test	Chaotic Map (2)	Chaotic Map (3)
Birthday spacing	0.8028 (✓)	0.6806 (✓)
Overlapping permutation	0.5354 (✓)	0.7975 (✓)
Binary rank 32×32	0.8732 (✓)	0.5353 (✓)
Binary rank 6×8	0.9177 (✓)	0.2626 (✓)
Bitstream	0.3148 (✓)	0.5024 (✓)
OPSO	0.7322 (✓)	0.1155 (✓)
OQSO	0.8579 (✓)	0.1203 (✓)
DNA	0.7211 (✓)	0.5940 (✓)
Count the ones 01	0.1000 (✓)	0.9094 (✓)
Count the ones 02	0.8106 (✓)	0.2239 (✓)
Parking lot	0.3937 (✓)	0.8578 (✓)
2DS sphere	0.3486 (✓)	0.0445 (✓)
3DS spheres	0.2722 (✓)	0.5457 (✓)
Squeeze	0.2749 (✓)	0.9096 (✓)
Overlapping sum	0.0566 (✓)	0.0445 (✓)
Runs	0.7123 (✓)	0.3845 (✓)
Craps	0.6480 (✓)	0.5095 (✓)

### C. Pseudo-Random Sequence Generation

Performing an XOR operation on an image with a pseudo-random sequence requires that each sequence value fall within the 0-255 range, corresponding to an 8-bit binary system. The pseudo-random sequence generation scheme introduced in this study reduces the iteration count of the chaotic sequence and consequently reduces the running time of sequence generation. The proposed scheme generates a single sequence by iterating only  $\frac{m \times n}{8}$  times, resulting in a total of  $\frac{m \times n}{4}$  iterations to generate the complete pseudo-random sequence.

- 1) Iterate two chaotic sequences of length  $\frac{m \times n}{8}$ , using the current timestamp as  $y_0$ , based on two novel 1D chaotic maps (2) and (3), respectively.
- 2) Each element of the chaotic sequence is treated as a 64-bit binary number and is subsequently divided into eight segments. These segments form the eight elements of the new pseudo-random sequence.

We utilize one of the chaotic systems to demonstrate the algorithm for generating pseudo-random sequences.

### D. Encryption and Decryption Algorithm

To reduce computational complexity and decrease running time, we employ an encryption scheme based on novel 1D chaotic maps. As illustrated in Fig. 4, the scheme encompasses five stages: sequence generation, sequence processing, reading, XOR operation, and writing.

- 1) Generate two pseudo-random sequences of length  $m \times n$ , utilizing novel 1D chaotic systems (2) and (3).
- 2) Execute an XOR operation between the two pseudo-random sequences.
- 3) Expand the processed chaotic sequence into three channels and fill in an encrypted matrix pixel by pixel.
- 4) Record the values of  $m$ ,  $n$ , timestamp, and the frame rate of the video into a new binary file.
- 5) Extract the original image from each frame of the video.
- 6) Execute an XOR operation between the encrypted matrix and the original image.

### Algorithm 1 Pseudo-Random Sequence Generation

---

```

1: function GENERATE_CHAOS_SEQUENCE( $m, n, t$ )
2:    $y_{next} \leftarrow t$ 
3:    $index \leftarrow 0$ 
4:   for  $i \leftarrow 0$  to  $\frac{m \times n}{8} - 1$  do
5:     for  $h \leftarrow 0$  to 7 do
6:        $Array[index] \leftarrow y_{next}[8 \times h : 8 \times h + 7]$ 
7:        $index \leftarrow index + 1$ 
8:     end for
9:      $y \leftarrow y_{next}$ 
10:    if  $i \% 2 == 0$  then
11:       $y_{next} \leftarrow ((\frac{y}{2^{32}} + 1) \times ((y \% 2^{32}) + 1) + 1)$ 
12:    else
13:       $y_{next} \leftarrow (y \ll (y \% 64)) \mid (y \gg (64 -$ 
14:         $(y \% 64)))$ 
15:    end if
16:  end for
17:  return  $Array$ 

```

---

- 7) Store each pixel of the encrypted gray image into a binary file.

### Algorithm 2 Encryption Algorithm

Input: Original Video ( $video$ )

Output: Encrypted File ( $outFile$ )

---

```

1:  $m \leftarrow GET(video, FRAME\_HEIGHT)$ 
2:  $n \leftarrow GET(video, FRAME\_WIDTH)$ 
3:  $t \leftarrow getCurrentTimestamp()$ 
4:  $c1 \leftarrow GENERATE\_CHAOS\_SEQUENCE1(m, n, t)$ 
5:  $c2 \leftarrow GENERATE\_CHAOS\_SEQUENCE2(m, n, t)$ 
6:  $c \leftarrow BITWISE\_XOR(c1, c2)$ 
7:  $En\_Mat \leftarrow EXPANDTORGB(c)$ 
8:  $frameRate \leftarrow GET(video, FPS)$ 
9:  $WRITE(outFile, m, n, frameRate, t)$ 
10:  $frameDataSize \leftarrow m \times n$ 
11: while  $READ(video, frame)$  do
12:    $En\_f \leftarrow BITWISE\_XOR(En\_Mat, frame)$ 
13:    $WRITE(outFile, En\_f.data, frameDataSize)$ 
14: end while
15:  $CLOSE(outFile)$ 
16:  $RELEASE(video)$ 

```

---

The decryption scheme is essentially the inverse of the encryption scheme, and the decrypted frames are stored in the video.

- 1) Extract the video size, timestamp and video frame rate from the received binary file.
- 2) Using the timestamp as the initial value, Generate two pseudo-random sequences of length  $m \times n$ , utilizing novel 1D chaotic systems (2) and (3).
- 3) Execute an XOR operation between the two pseudo-random sequences.
- 4) Expand the processed chaotic sequence into three channels and fill in an decrypted matrix pixel by pixel.
- 5) Retrieve each encrypted frame from the binary file.

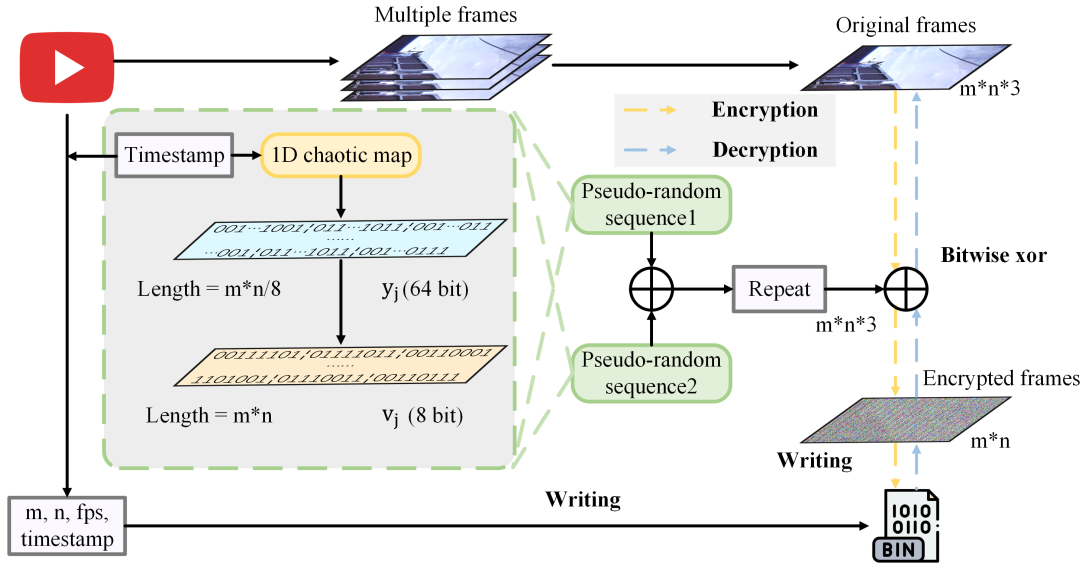


Fig. 4. Encryption process of the proposed algorithm.

- 6) Execute an XOR operation between the decrypted matrix and the encrypted image.
- 7) Encode each frame of the decrypted image into the decrypted video.

#### E. Satellite Video Communication Framework

The upper part of Fig. 1 demonstrates the satellite video communication framework we adopted. Satellite video communication usually consists of three components: video capture, encryption, and data transmission. In this process, video data is captured by the satellite payload and generates a raw video stream. Subsequently, this video data is encrypted in real time by the proposed encryption scheme to ensure the security of the data during transmission. The encrypted data is saved as a binary file and then transmitted to the ground station through a satellite communication link.

#### F. Experiments on a Satellite

The experiment utilized a satellite payload on the Tiansuan Constellation platform, which is a Raspberry Pi 4B equipped with a 1.5GHz CPU. We tested the full time of running the encryption algorithm on the satellite and compared it with the experiment on the ground. The tests were conducted using two video samples: a 30s 360p video and a 10s 720p video, both recorded at 20 FPS. The experimental results are presented in Tab. II.

In addition, we obtained the encrypted binary file from the satellite for decryption and found that our encryption results did not lose data and could be completely restored to the original video. To protect the privacy of the brand in the advertisement, Fig. 5 displays cropped frames from the decrypted video. The experimental data on Tab. II and Fig. 5 are provided by the Tiansuan Constellation platform.

It can be observed that the encryption time in each experiment is shorter than the duration of the original video, although the experimental data on the satellite shows slightly

greater fluctuations compared to that on the ground. This may be attributed to temperature variations and power efficiency instability during satellite operation. Nevertheless, despite occasional performance instability, the experimental results remain largely consistent with those on the ground, demonstrating the capability for real-time encryption.

TABLE II  
COMPARISON OF EXPERIMENTS IN SPACE AND ON THE GROUND.

Number of experiments	Experiments in space		Experiments on the ground	
	360p	720p	360p	720p
1	2.2629	2.8187	2.2534	2.7189
2	2.4708	2.6597	2.2703	2.6462
3	2.2378	2.7568	2.3441	2.6731
4	2.2432	2.6597	2.2793	2.6983
5	2.2670	2.6727	2.2484	2.6766
<b>95% Interval Confidence</b>	2.2963 ±0.0400	2.7135 ±0.0658	2.2791 ±0.0338	2.6827 ±0.0239

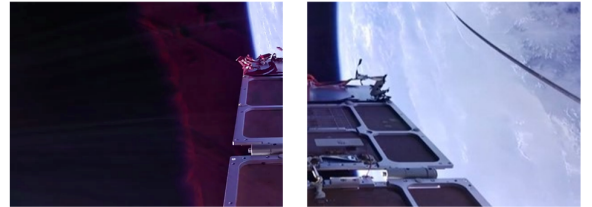


Fig. 5. Cropped frames after decrypting binary file from satellite.

#### G. FPGA Implementation

Field Programmable Gate Array (FPGA) is a flexible programmable hardware platform with powerful parallel processing capabilities, which is suitable for implementing real-time and efficient digital signal processing and encryption algorithm applications. In order to ensure that our encryption scheme can be deployed on different edge devices, we deployed

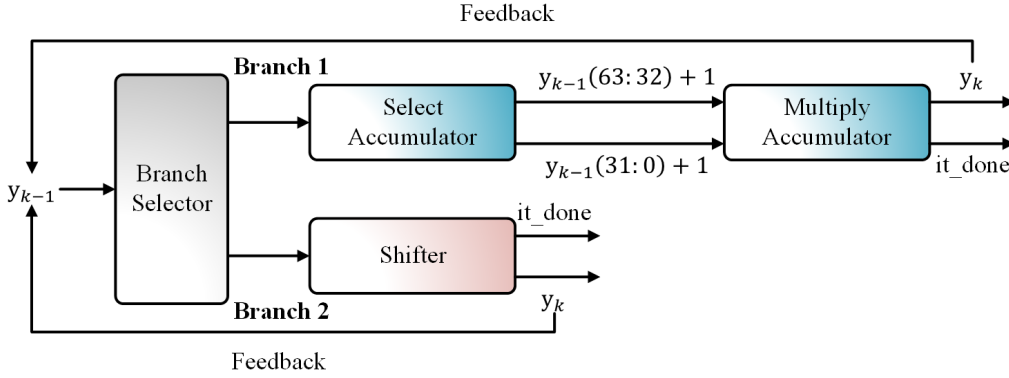


Fig. 6. Block diagram of hardware architecture for the proposed chaotic map.

the proposed chaotic sequence generation scheme to Xilinx FPGA-Zynq xc020clg484. In this work, we used the Vivado 2018.3 version. First, we designed the IP core in the Vivado High-Level Synthesis (HLS) environment and imported the C++ code into the HLS project. To verify the correctness of the design, we also added a test bench file and used the Vivado HLS built-in simulator to perform a comprehensive functional simulation of the IP core. Subsequently, we perform synthesis and implement operations in sequence to convert the C++ code into a Verilog description and map the generated bitstream to the target FPGA device. Finally, the final deployment of the hardware circuit is achieved.

Fig. 6 shows a simple block diagram of the chaotic map. In the hardware architecture of the chaotic map, the system has only one input  $y_{k-1}$ , which represents the state value of the previous iteration. The design first uses a Branch Selector module, which determines the data path according to the value of the current iteration index  $k$ . In Branch 1, the Select Accumulator module uses the registers and arithmetic units in the FPGA to process the upper 32 bits and lower 32 bits of the 64-bit input  $y_{k-1}$ , respectively, where  $y_{k-1}(63:32) + 1$  corresponds to  $\frac{y_{k-1}}{2^{32}} + 1$ , and  $y_{k-1}(31:0) + 1$  corresponds to  $y_{k-1} \% 2^{32} + 1$ . The design replaces division and remainder operations with shift operations, making full use of the efficient shift registers of the FPGA, thereby significantly improving the operation speed and resource utilization. In the next Multiply Accumulator module, the two outputs of the previous module are multiplied and added by 1 using a multiplier and an adder. On the other hand, in Branch 2, the Shifter module implements a circular shift on the 64-bit input  $y_{k-1}$ . The module first determines the shift amount by intercepting the lower 6 bits  $y_{k-1}(5:0)$ , then uses the left shift (shift amount) and right shift ( $64 - \text{shift amount}$ ) operations to split  $y_{k-1}$  into two parts, and finally merges the two parts of the result through a bitwise OR operation. The system generates  $y_k$  as the result of the current iteration of the chaotic map, which is saved by the register and feedback as the input  $y_{k-1}$  of the next iteration. In addition, the status register generates an iteration completion signal *it\_done* to indicate the end of this operation cycle.

Fig. 7 shows the overall framework diagram.

Fig. III shows the 10 simulation results of the proposed chaotic mapping in hexadecimal format on different edge

devices. It can be seen that our chaotic system can achieve consistent simulation results on any hardware platform.

TABLE III  
COMPARISON OF SIMULATION RESULTS FOR TWO CHAOTIC MAPS ON  
FPGA AND RASPBERRY PI PLATFORMS UNDER IDENTICAL INITIAL  
VALUES.

Chaotic Map (2)		Chaotic Map (3)	
Pi	FPGA	Pi	FPGA
759800000033e4a	759800000033e4a	0844581288ce6a18	0844581288ce6a18
00017d65438b3e4c	00017d65438b3e4c	1288ce6a18084458	1288ce6a18084458
17d65438b3e4c000	17d65438b3e4c000	01bd6c9343bc2f34	01bd6c9343bc2f34
10c029a7b4c5143a	10c029a7b4c5143a	f3401bd6c9343bc2	f3401bd6c9343bc2
e84300a69ed31450	e84300a69ed31450	02baa010501ffd89	02baa010501ffd89
0902c716f3b85529	0902c716f3b85529	754020a03ffb1205	754020a03ffb1205
70aa5212058e2de7	70aa5212058e2de7	1d4dc628dea715c7	1d4dc628dea715c7
0271e647f051b839	0271e647f051b839	a6e3146f538ae38e	a6e3146f538ae38e
7204e3cc8fe0a370	7204e3cc8fe0a370	3c0832623be29e20	3c0832623be29e20
4014c8524794147e	4014c8524794147e	3be29e203c083262	3be29e203c083262

#### IV. PERFORMANCE AND SECURITY ANALYSIS

To assess the effectiveness of real-time video encryption on satellite payloads, we conducted two types of analyses: (a) performance analysis and (b) security analysis. All experiments were conducted on a Raspberry Pi 4B, which is based on the Broadcom BCM2711 SoC and integrates a quad-core Cortex-A72 (ARM v8) 64-bit processor operating at 1.5GHz, 8GB LPDDR4-3200 SDRAM, and 64GB SD card storage, running a 64-bit Raspberry Pi OS.

Fig. 8 displays randomly selected frames from the original, encrypted, and decrypted videos.

##### A. Time Analysis

We considered two application scenarios: (a) One scenario includes the complete encryption process, including five stages: sequence generation, sequence processing, reading, XOR operation, and writing. (b) The second scenario only considers the encryption algorithm. In our algorithm, the encryption process is only one XOR. Our design takes into account the requirement of different application scenarios, considering both the performance evaluation of the complete

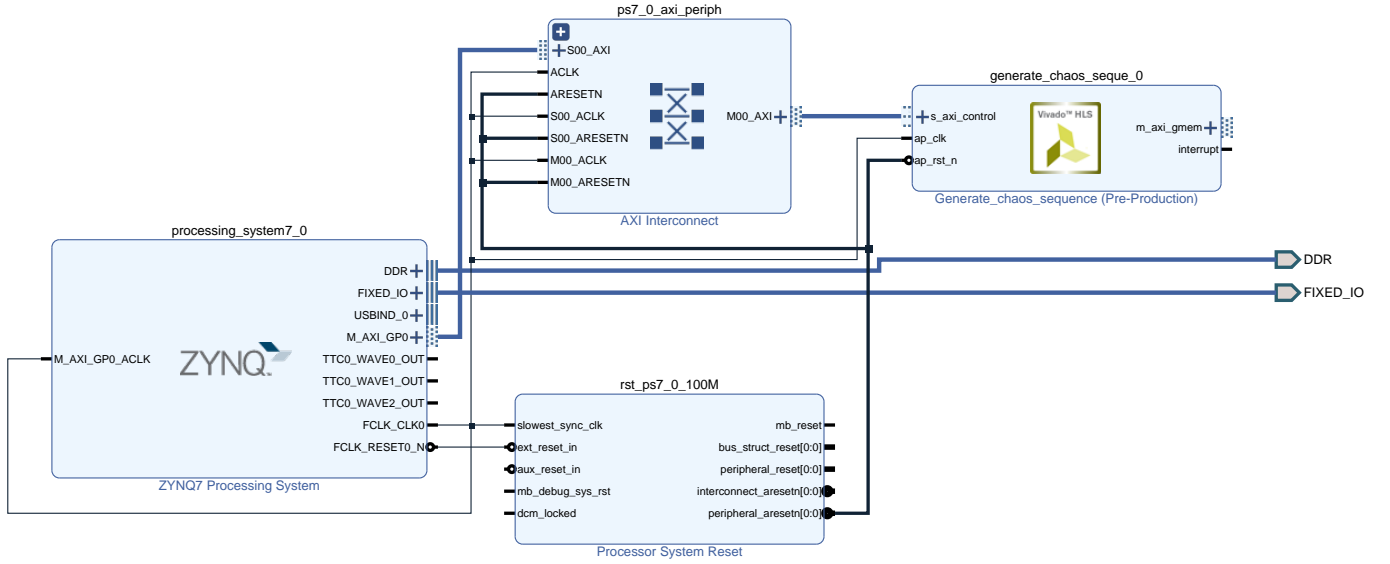


Fig. 7. The architecture diagram through Vivado simulation.

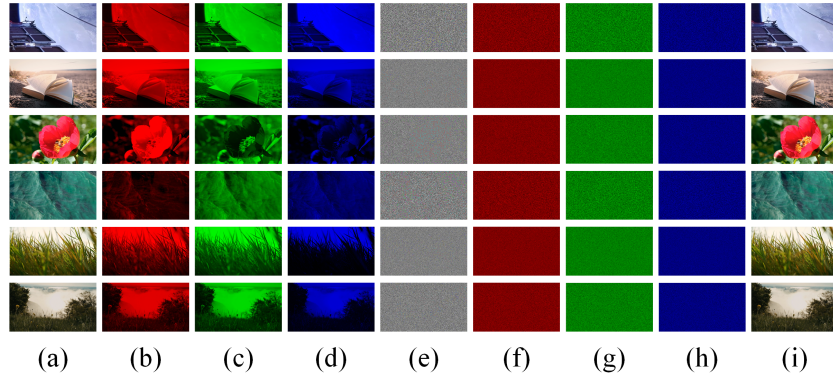


Fig. 8. Video frames: (a,b,c,d) original images and their R, G, B channels, (e,f,g,h) encrypted images and their R, G, B channels, (i) decrypted images.

process to adapt to the performance bottleneck in practical applications and the high efficiency requirements in lightweight encryption scenarios.

Tab. IV presents the total encryption times and 95% confidence intervals for eight videos. The results indicate that this scheme can encrypt up to 1K resolution videos while maintaining excellent real-time performance. During the experiments, it was observed that video reading and writing accounted for the majority of the processing time. To address this problem, we adopted a strategy of writing to binary files, significantly reducing write time and enhancing the real-time capability of the complete encryption process.

Tab. V lists the encryption times of the proposed algorithm and compares them with other algorithms. The bolded values in the table highlight the best results in terms of encryption time. The results show that, when considering only the encryption process, the proposed scheme can encrypt videos with resolutions up to 2K. Furthermore, compared to other algorithms, our method demonstrates faster encryption speeds and is more suitable for embedded devices with limited computational capabilities.

TABLE IV  
ENCRYPTION TIME OF THE COMPLETE ENCRYPTION PROCESS.

Video	Width	Height	FPS	Original video duration	Encrypted time
1	640	360	20	30	2.3428 ± 0.0924
2	640	360	29.97	13	1.6247 ± 0.0467
3	1280	720	29.97	13	5.4627 ± 0.0568
4	960	540	23.98	40	7.7184 ± 0.0563
5	960	540	30	30	6.9647 ± 0.0470
6	640	360	30	30	3.3859 ± 0.0310
7	1280	720	24	19	6.7034 ± 0.0412
8	960	540	25	18	3.6928 ± 0.0657
9	1920	1080	29.97	11	10.9255 ± 0.0715

### B. Power Consumption Analysis

In the context of satellite communication systems, both the reliability and operational longevity of satellite devices are extremely critical. Given the high maintenance and energy supply costs associated with satellite payloads, conducting a power consumption analysis becomes necessary to ensure that the encryption algorithms employed do not surpass the

TABLE V  
COMPARISON OF ENCRYPTION ALGORITHM TIME WITH DIFFERENT ALGORITHMS.

Video	Width	Height	FPS	Original video duration	Encrypted time					
					AES	Ref. [22]	Ref. [23]	Ref. [18]	Ref. [24]	Proposed
7	1280	720	24	19	19.5309	82.3405	20.9101	23.2585	40.3472	<b>1.6955 ± 0.0147</b>
8	960	540	25	18	10.6195	69.9457	10.5545	12.6043	20.3263	<b>0.8846 ± 0.0077</b>
9	1920	1080	29.97	11	30.4775	138.847	29.0570	36.3955	58.4864	<b>3.2532 ± 0.0741</b>
10	1920	1020	24	26	58.5893	266.634	57.0904	70.4209	111.2180	<b>5.8099 ± 0.0198</b>
11	2560	1440	30	30	148.728	713.092	152.7620	177.473	284.662	<b>15.3312 ± 0.3554</b>
12	3840	2160	29.62	5	57.4345	321.101	54.5954	68.7311	108.892	<b>5.2975 ± 0.0824</b>

allotted resource budget. Excessive power consumption not only threatens to reduce the operating life of the device but may also lead to overheating, thereby jeopardizing the security and real-time performance of the encryption algorithm in satellite communication applications.

To assess the power consumption characteristics of the proposed encryption algorithm, we employed the IoT Power CC device to measure power usage on a Raspberry Pi 4B, effectively simulating an embedded system environment representative of satellite payload constraints. Fig. 9 illustrates the power consumption before and during encryption, along with a comparison of the performance of other algorithms. Specifically, Algorithms 1, 2, 3, 4, and 5 correspond to Ref. [22], Ref. [23], Ref. [18], Ref. [24], and the AES algorithm, respectively. As shown, most algorithms maintain power consumption levels around 2.6W. However, due to slower encryption speeds, some algorithms occasionally exhibit lower power consumption, dropping to approximately 2.4W. In contrast, our proposed algorithm rarely demonstrates such lower power levels, attributed to its higher encryption efficiency. Overall, the power consumption of our algorithm remains stable and is not significantly higher than that of the other algorithms.

### C. Key space analysis

An effective encryption system requires a large key space that can successfully withstand attacks [25]. According to cryptographic standards, the key space of a secure system should not be smaller than  $2^{100}$  to effectively resist brute-force attacks [26]. Due to the 64-bit initial value  $y_0$  of the proposed novel 1D chaotic map, the key space of the system is  $2^{64} \times 2^{64} = 2^{128}$ . This key space is large enough to withstand brute-force attacks.

### D. Histogram Analysis

Histogram analysis is employed to ascertain the distribution of pixel values in a particular image [27]. Fig. 10 displays histograms of the R, G, and B channels in both the original picture and the encrypted image.

The dissimilarity between the histograms of the encrypted image and the original image is apparent. The encrypted histograms of the R, G, and B channels have a smooth distribution, suggesting excellent encryption performance.

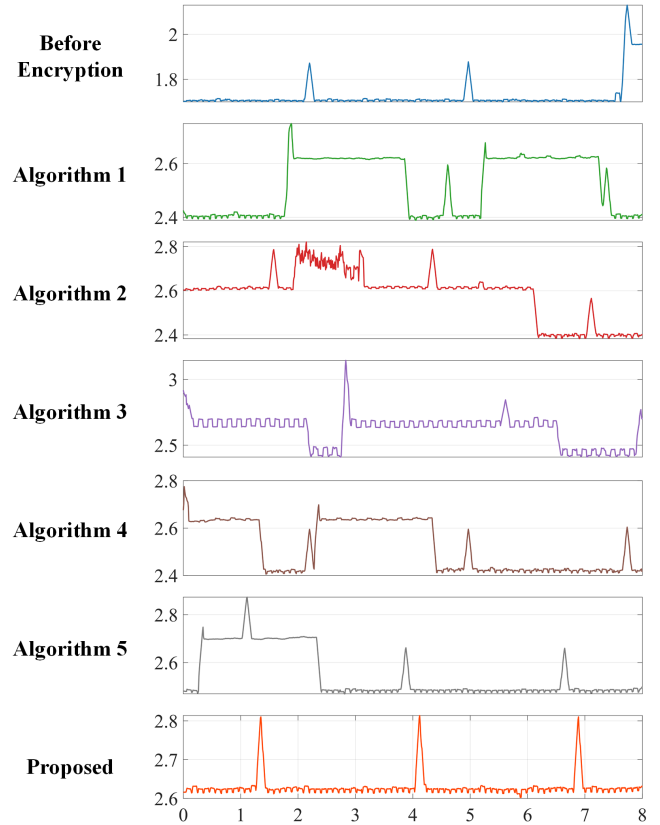


Fig. 9. Power (W) waveforms before and after the encryption scheme is executed, and the comparison with different algorithms.

### E. Information Entropy Analysis

Entropy is a useful statistic for measuring the level of randomness. The information entropy approaches 8, indicating that the encryption technique is robust and secure [28]. The calculation is performed as follows:

$$H(k) = - \sum_{i=0}^{2^n-1} p(k_j) \log_2(p(k_j)) \quad (4)$$

where the probability of the symbol  $k_j$  is denoted by  $p(k_j)$ . Tab. VI shows information entropy for six images.

The table shows that the information entropy closely aligns with the predicted value, suggesting that the technique is



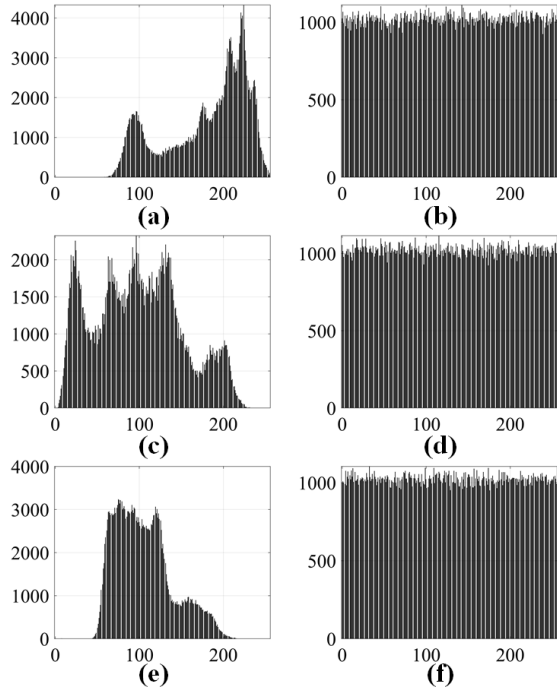


Fig. 10. Histograms of the original image and the encrypted image: (a,b) R channel, (c,d) G channel, (e,f) B channel.

TABLE VI  
RESULTS OF INFORMATION ENTROPY ANALYSIS.

Image	Size	Original images	Encrypted images
1	640 × 360	7.2723	7.9997
2	1280 × 720	7.8131	7.9999
3	960 × 540	7.4944	7.9998
4	640 × 360	6.8443	7.9997
5	1280 × 720	7.7089	7.9999
6	960 × 540	7.4357	7.9999

effective in defending against entropy attacks [29]. Tab. VII presents a comparison of the proposed encryption algorithm with other encryption algorithms for a  $512 \times 512$  Lena image. The results show that the entropy achieved by our algorithm is closer to the ideal value, demonstrating superior performance.

#### F. Correlation Analysis

The correlation quantifies the association between adjacent pixels in the image [30]. Images with a high correlation are easier to crack, whereas images with a low correlation are more difficult to distinguish [31]. The correlation coefficients are defined as:

$$\left\{ \begin{array}{l} \mu(u) = \frac{1}{M} \sum_{j=1}^M u_j \\ \sigma^2(u) = \frac{1}{M} \sum_{j=1}^M (u_j - \mu(u))^2 \\ \kappa(u, v) = \frac{1}{M} \sum_{j=1}^M (u_j - \mu(u))(v_j - \mu(v)) \\ \rho(u, v) = \frac{\kappa(u, v)}{\sigma(u)\sigma(v)} \end{array} \right. \quad (5)$$

TABLE VII  
COMPARISON OF INFORMATION ENTROPY WITH DIFFERENT ALGORITHMS.

Algorithm	Entropy
Ref. [22]	7.9994
Ref. [23]	7.9994
Ref. [18]	7.9991
Ref. [14]	7.9985
Ref. [32]	7.9977
Ref. [33]	7.9975
Ref. [34]	7.9993
Ref. [35]	7.9994
Proposed	<b>7.9998</b>

where  $u$  and  $v$  represent two adjacent pixels in the horizontal, vertical, and diagonal directions. The correlation analysis results for six images are presented in Tab. VIII, which shows the pixel value correlation.

TABLE VIII  
RESULTS OF CORRELATION ANALYSIS.

Image	Size	Channels	Original images			Encrypted images		
			Horiz.	Vert.	Diag.	Horiz.	Vert.	Diag.
1	640	R	0.9924	0.9916	0.9890	-0.0035	0.0033	-0.0042
	×	G	0.9943	0.9936	0.9917	-0.0018	0.0035	-0.0039
	360	B	0.9949	0.9940	0.9923	-0.0040	0.0019	0.0005
2	1280	R	0.9987	0.9971	0.9963	0.0054	0.0023	0.0006
	×	G	0.9988	0.9971	0.9965	0.0045	0.0024	0.0007
	720	B	0.9986	0.9967	0.9961	0.0040	0.0034	0.0011
3	960	R	0.9966	0.9970	0.9933	-0.0013	0.0027	-0.0005
	×	G	0.9910	0.9911	0.9820	-0.0008	0.0041	0.0003
	540	B	0.9887	0.9887	0.9766	-0.0004	0.0038	-0.0008
4	640	R	0.9799	0.9752	0.9657	0.0039	0.0042	0.0018
	×	G	0.9856	0.9841	0.9770	0.0024	0.0027	0.0006
	360	B	0.9791	0.9763	0.9656	0.0014	0.0027	0.0037
5	1280	R	0.9828	0.9949	0.9881	-0.0002	0.0029	-0.0024
	×	G	0.9815	0.9945	0.9873	-0.0010	0.0032	-0.0016
	720	B	0.9861	0.9958	0.9902	0.0001	0.0031	-0.0017
6	960	R	0.9954	0.9977	0.9935	-0.0010	0.0027	-0.0008
	×	G	0.9952	0.9977	0.9934	-0.0005	0.0023	-0.0001
	540	B	0.9955	0.9978	0.9938	-0.0002	0.0036	0.00002

The correlations in the proposed method are noticeably lower compared to the original images [36]. Tab. IX compares the correlation results of the Lena image encrypted by different algorithms and the proposed algorithm. It can be observed that our encryption algorithm achieves relatively low correlation values across all three directions, with three indices being the lowest among the comparisons.

Fig. 11 and Fig. 12 display the correlation distributions of the adjacent pixels in the R, G, and B channels for the original

TABLE IX  
COMPARISON OF CORRELATION WITH DIFFERENT ALGORITHMS.

Algorithm	Channels	Correlation		
		Horiz.	Vert.	Diag.
Ref. [22]	R	0.0031	0.0080	0.0043
	G	-0.0029	-0.00002	<b>-0.0014</b>
	B	0.0035	-0.0057	<b>0.0004</b>
Ref. [18]	R	-0.0032	<b>-0.0009</b>	-0.0031
	G	0.0044	<b>-0.0003</b>	0.0019
	B	-0.0034	-0.0008	0.0027
Ref. [37]	R	0.0011	-0.0098	-0.0071
	G	<b>-0.0025</b>	-0.0120	-0.0090
	B	0.0003	-0.0082	-0.0065
Ref. [38]	R	-0.0050	-0.0096	0.0018
	G	<b>0.0025</b>	-0.0032	0.0015
	B	0.0035	-0.0023	-0.0042
Ref. [39]	R	-0.0045	0.0149	-0.0033
	G	0.0026	0.0126	-0.0013
	B	<b>-0.0001</b>	0.0074	0.0021
Proposed	R	<b>-0.0004</b>	0.0014	<b>-0.0003</b>
	G	-0.0050	-0.0006	-0.0032
	B	-0.0032	<b>-0.0006</b>	-0.0006

and encrypted pictures in diagonal, horizontal, and vertical directions, respectively.

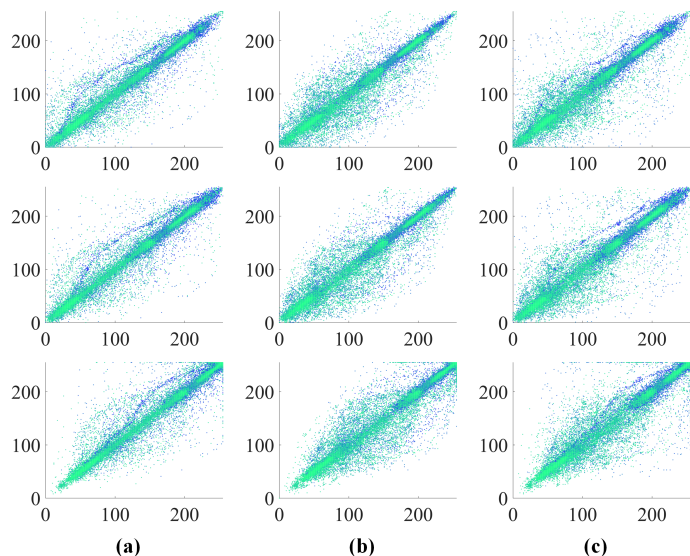


Fig. 11. Correlation analysis of the original images of the R, G, B channels: (a) horizontal direction, (b) vertical direction, (c) diagonal direction.

The results show strong correlations in the original image, which are significantly decreased after encryption, indicating that the proposed algorithm can effectively resist statistical attacks.

### G. Differential Attack Analysis

In order to defend against a differential attack, a secure encryption method must demonstrate susceptibility to minor alterations within the original image. Thus, every alteration of a single bit in the original image should cause the encryption process to produce an entirely distinct encrypted image [40]. The computation of NPCR and UACI is determined according to the following formula:

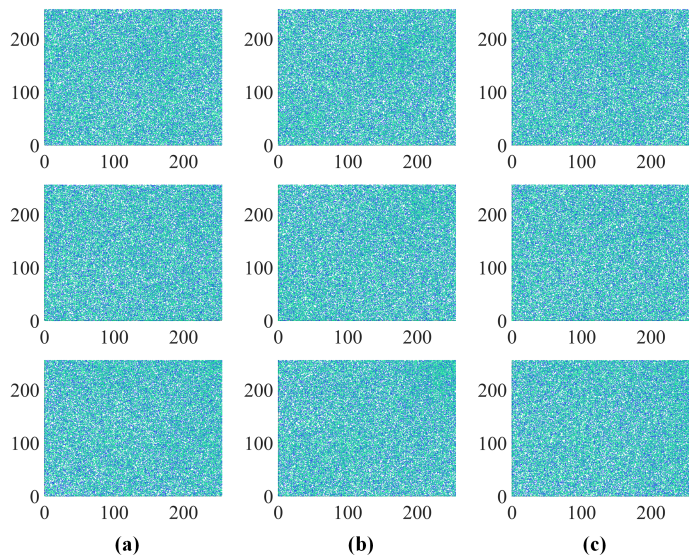


Fig. 12. Correlation analysis of the encrypted images of the R, G, B channels: (a) horizontal direction, (b) vertical direction, (c) diagonal direction.

$$\begin{cases} \Delta_{nm} = |C_1(n, m) - C_2(n, m)| \\ \text{NPCR} = \frac{100\%}{MN} \sum_{n=1}^N \sum_{m=1}^M \text{sign}(\Delta_{nm}) \\ \text{UACI} = \frac{100\%}{TMN} \sum_{n=1}^N \sum_{m=1}^M \Delta_{nm} \end{cases} \quad (6)$$

where  $C_1$  and  $C_2$  represent two encrypted images of size  $M \times N$ , with  $T$  denoting the maximum permissible pixel intensity. The theoretical values of NPCR and UACI are 99.6094% and 33.4635%, respectively. After subtracting the encrypted images, the resulting images in Fig. 13 show a substantial difference.

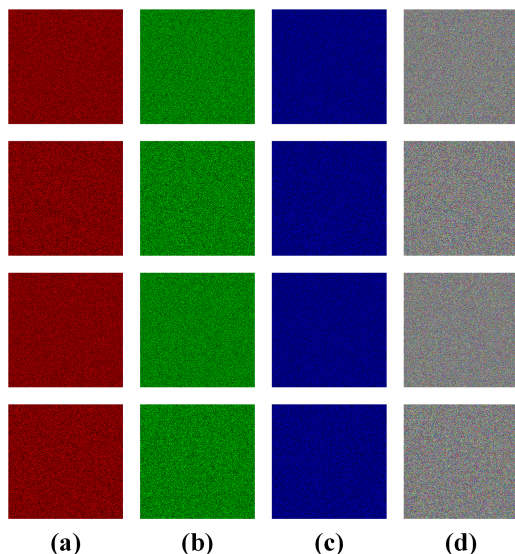


Fig. 13. Differential attack analysis: (a) R channel, (b) G channel, (c) B channel, (d) combined images.

Tab. X presents the NPCR and UACI values in the context of differential attack analysis. Tab. XI shows the comparison results of the proposed algorithm and other algorithms. It has been observed that the NPCR and UACI values are near the theoretical values. Therefore, the proposed algorithm demonstrates sensitivity to even minor variations in input images.

TABLE X  
NPCR AND UACI OF THREE CHANNELS IN DIFFERENTIAL ATTACK ANALYSIS.

Image	Size	NPCR(%)			UACI(%)		
		R	G	B	R	G	B
1	640 × 360	99.6007	99.6007	99.6007	33.4600	33.4181	33.4215
2	1280 × 720	99.6055	99.6055	99.6055	33.5319	33.4693	33.4361
3	960 × 540	99.6190	99.6190	99.6190	33.3859	33.4021	33.4368
4	640 × 360	99.5981	99.5981	99.5981	33.4310	33.4450	33.4540
5	1280 × 720	99.5947	99.5947	99.5947	33.4711	33.4814	33.4958
6	960 × 540	99.6154	99.6154	99.6154	33.4482	33.4350	33.4233

TABLE XI  
COMPARISON OF NPCR AND UACI IN DIFFERENTIAL ATTACK ANALYSIS.

Algorithm	NPCR(%)	UACI(%)
Ref. [22]	99.6286	33.4669
Ref. [23]	99.61	33.48
Ref. [18]	99.63	33.52
Ref. [14]	99.61	33.43
Ref. [32]	99.6338	33.5048
Ref. [33]	99.6147	33.4723
Ref. [34]	99.6089	33.4619
Ref. [35]	99.6006	33.4295
Proposed	99.6071	33.4654

### H. Key Sensitive Analysis

In order to enhance the security of an encryption algorithm against brute force assaults, it is crucial for the algorithm to demonstrate a high level of sensitivity to even the slightest modifications in the secret key [41]. By making a little change to the original key value using just one binary bit, the key shows noticeable variations. Fig. 14 depicts the temporal waveform of the original key and the altered key, as well as their disparities. Fig. 15 displays the results of the key sensitive experiments.

Tab. XII presents the NPCR and UACI values in the key sensitivity analysis. Tab. XIII demonstrates the comparison results of the proposed algorithm and other algorithms. The calculated values of NPCR and UACI closely approximate their respective theoretical values, demonstrating the proposed algorithm exhibits high sensitivity to changes in the key.

### I. Ablation Analysis

In the ablation experiments, we tested the proposed scheme using only a single chaotic sequence, referred to as the Only Chaotic sequence (2) (OC2) and the Only Chaotic sequence (3) (OC3). Additionally, since the generated sequences are identical across the R, G, and B channels, we also tested a scheme that generates a pseudo-random sequence of length

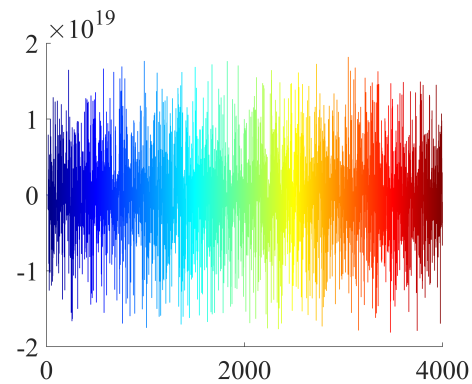


Fig. 14. The difference waveform of two keys over time.

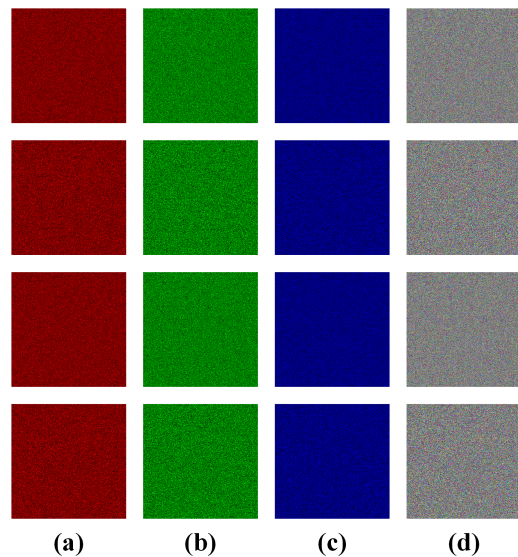


Fig. 15. Key sensitivity analysis: (a) R channel, (b) G channel, (c) B channel, (d) combined images.

TABLE XII  
NPCR AND UACI OF THREE CHANNELS IN KEY SENSITIVE ANALYSIS.

Image	Size	NPCR(%)			UACI(%)		
		R	G	B	R	G	B
1	640 × 320	99.6120	99.6120	99.6120	33.4879	33.4846	33.4306
2	1280 × 720	99.6212	99.6212	99.6212	33.5341	33.4856	33.4512
3	960 × 540	99.6078	99.6078	99.6078	33.4882	33.4967	33.5075
4	640 × 360	99.6085	99.6085	99.6085	33.4979	33.4818	33.4700
5	1280 × 720	99.6110	99.6110	99.6110	33.4418	33.4475	33.4427
6	960 × 540	99.6035	99.6035	99.6035	33.4803	33.4763	33.4969

TABLE XIII  
COMPARISON OF NPCR AND UACI IN KEY SENSITIVE ANALYSIS.

Algorithm	NPCR(%)	UACI(%)
Ref. [18]	99.60	33.44
Ref. [35]	99.5999	33.5060
Ref. [37]	99.612	33.468
Ref. [39]	99.61	33.78
Proposed	99.6052	33.4654

$\frac{3 \times m \times n}{8}$ , referred to as 3L. Tab. XIV shows the ablation analysis result.

TABLE XIV  
RESULTS OF ABLATION ANALYSIS.

Algorithm	NPCR(%)	UACI(%)	Correlation		
			Horiz.	Vert.	Diag.
OC2	99.4781	32.0991	0.0015	0.0437	0.0013
OC3	99.4476	32.1821	<b>-0.0006</b>	0.0439	0.0029
3L	99.5999	33.4706	-0.0028	0.0052	<b>-0.0001</b>
Proposed	<b>99.6071</b>	<b>33.4654</b>	-0.0028	<b>0.0039</b>	-0.0013

It can be observed that when only a single chaotic sequence is used, the encrypted images exhibit higher vertical correlation, and the NPCR and UACI values are less ideal compared to the proposed scheme. Furthermore, using a pseudo-random sequence three times longer does not result in significantly improved encryption performance. Considering both efficiency and security, we chose the proposed encryption scheme.

### J. NIST Test

We have chosen the NIST test suite to assess the unpredictability of the data. The analysis consists of 15 tests to fulfill crucial requirements [42]. In order to pass the test, the p-value must exceed 0.01. The test result of an encrypted image is shown in Tab. XV, demonstrating the effectiveness of the proposed encryption method.

TABLE XV  
RESULT OF NIST TESTS SUITE.

Test	p-Value	Assessment
ApproximateEntropy	0.213309	SUCCESS
BlockFrequency	0.350485	SUCCESS
CumulativeSums	0.739918	SUCCESS
FFT	0.066882	SUCCESS
Frequency	0.213309	SUCCESS
LinearComplexity	0.213309	SUCCESS
LongestRun	0.350485	SUCCESS
NonOverlappingTemplate	0.999438	SUCCESS
OverlappingTemplate	0.739918	SUCCESS
RandomExcursions	0.637119	SUCCESS
RandomExcursionsVariant	0.834308	SUCCESS
Rank	0.834308	SUCCESS
Runs	0.911413	SUCCESS
Serial	0.991468	SUCCESS
Universal	0.122325	SUCCESS

### K. DIEHARD test

Tab. XVI reveals the DIEHARD test result of an encrypted image, indicating that the encrypted image exhibits highly random behavior.

## V. CONCLUSION

Implementing real-time video encryption on satellite embedded systems is essential for improving the security and dependability of satellite communications. Utilizing existing video encryption systems on satellite payloads presents obstacles such as real-time performance and limited computing

TABLE XVI  
RESULT OF DIEHARD TESTS SUITE.

Test	p-Value	Assessment
Birthday spacing	0.3533	PASSED
Overlapping permutation	0.7423	PASSED
Binary rank 32×32	0.3813	PASSED
Binary rank 6×8	0.2534	PASSED
Bitstream	0.8643	PASSED
OPSO	0.9603	PASSED
OQSO	0.0897	PASSED
DNA	0.9930	PASSED
Count the ones 01	0.3173	PASSED
Count the ones 02	0.4699	PASSED
Parking lot	0.9637	PASSED
2DS sphere	0.4767	PASSED
3DS spheres	0.5744	PASSED
Squeeze	0.2783	PASSED
Overlapping sum	0.1785	PASSED
Runs	0.7988	PASSED
Craps	0.6144	PASSED

resources. In contrast, this work presents a novel approach for encrypting videos based on 1D chaotic mapping, specifically designed to address these limitations. We deployed a real-time video encryption algorithm on a satellite for the first time, demonstrating exceptional performance. According to the results of the experiments, this approach exhibits robust real-time performance and requires low power consumption. Notably, while considering only the encryption scheme, the system is capable of processing 2K video in real time, demonstrating its applicability to high-resolution video scenarios. Furthermore, FPGA deployment verified that the chaotic mapping values are consistent with those obtained on a Raspberry Pi, confirming the method’s hardware feasibility and stability. Comprehensive security evaluations also confirmed the system’s capability to endure diverse attacks. In the future, we will explore the extension of this method to support higher-resolution videos and integrate the encryption scheme with real satellite applications to further validate its effectiveness and adaptability. It is expected that this study will advance the field of video streaming security for satellite embedded devices and lay a strong foundation for future advancements in secure, real-time data transmission in satellite communication systems.

## ACKNOWLEDGMENT

This study is supported by the Talent Scientific Fund of Lanzhou University. Experiments for this study were facilitated by the TianSuan Constellation Platform at Beijing University of Posts and Telecommunications.

Special thanks are extended to Professor Shangguang Wang at Beijing University of Posts and Telecommunications for his invaluable guidance and support. Appreciation is also due to PhD student Ruolin Xing and Master’s student Linshuo Song at Beijing University of Posts and Telecommunications for their significant contributions to the research.

## REFERENCES

- [1] Y. Li, M. Wang, K. Hwang, Z. Li, and T. Ji, “Leo satellite constellation for global-scale remote sensing with on-orbit cloud ai computing,” *IEEE*

- Journal of Selected Topics in Applied Earth Observations and Remote Sensing*, vol. 16, pp. 9369–9381, 2023.
- [2] S. Yang and S. Sun, "A video encryption method based on chaotic maps in dct domain," *Progress in Natural Science*, vol. 18, no. 10, pp. 1299–1304, 2008.
  - [3] C. Liu, H. Zhang, W. Chen, and F. M. Ghannouchi, "Novel design space of broadband high-efficiency parallel-circuit class-ef power amplifiers," *IEEE Transactions on Circuits and Systems I: Regular Papers*, vol. 69, no. 9, pp. 3465–3475, 2022.
  - [4] D. Jiang, Z. Yuan, W.-x. Li, H.-t. Wang, and L.-l. Lu, "Real-time chaotic video encryption based on multi-threaded parallel confusion and diffusion," *Information Sciences*, vol. 666, p. 120420, 2024.
  - [5] M. S. Azzaz, C. Tanougast, A. Maali, and M. Benssalah, "An efficient and lightweight multi-scroll chaos-based hardware solution for protecting fingerprint biometric templates," *International Journal of Communication Systems*, vol. 33, no. 10, p. e4211, 2020.
  - [6] M. A. Hadjadj, S. Sadoudi, M. S. Azzaz, H. Bendecheche, and R. Kaibou, "A new hardware architecture of lightweight and efficient real-time video chaos-based encryption algorithm," *Journal of Real-Time Image Processing*, vol. 19, no. 6, pp. 1049–1062, 2022.
  - [7] Y. Ali, Y. Xia, W. Sulek, and T. Manzoor, "Chaos-encryption-based secure polar coding for network-oriented cloud control system," *IEEE Transactions on Industrial Informatics*, vol. 20, no. 3, pp. 3935–3947, 2024.
  - [8] X. Liu, C. Li, S. S. Ge, and D. Li, "Time-synchronized control of chaotic systems in secure communication," *IEEE Transactions on Circuits and Systems I: Regular Papers*, vol. 69, no. 9, pp. 3748–3761, 2022.
  - [9] H. Bao, Z. Hua, H. Li, M. Chen, and B. Bao, "Discrete memristor hyperchaotic maps," *IEEE Transactions on Circuits and Systems I: Regular Papers*, vol. 68, no. 11, pp. 4534–4544, 2021.
  - [10] B. Vaseghi, S. S. Hashemi, S. Mobayen, and A. Fekih, "Finite time chaos synchronization in time-delay channel and its application to satellite image encryption in ofdm communication systems," *IEEE Access*, vol. 9, pp. 21 332–21 344, 2021.
  - [11] M. Ji'e, D. Yan, S. Sun, F. Zhang, S. Duan, and L. Wang, "A simple method for constructing a family of hamiltonian conservative chaotic systems," *IEEE Transactions on Circuits and Systems I: Regular Papers*, vol. 69, no. 8, pp. 3328–3338, 2022.
  - [12] C. Yang, X. Wei, and C. Wang, "S-box design based on 2d multiple collapse chaotic map and their application in image encryption," *Entropy*, vol. 23, no. 10, p. 1312, 2021.
  - [13] A. K. Singh, K. Chatterjee, and A. Singh, "An image security model based on chaos and dna cryptography for iiot images," *IEEE Transactions on Industrial Informatics*, vol. 19, no. 2, pp. 1957–1964, 2023.
  - [14] L. Zhao, L. Zhao, F. Cui, and T. Sun, "Satellite image encryption based on rna and 7d complex chaotic system," *The Visual Computer*, pp. 1–21, 2023.
  - [15] Y. Li, L. Liang, Z. Su, and J. Jiang, "A new video encryption algorithm for h. 264," in *2005 5th International Conference on Information Communications & Signal Processing*. IEEE, 2005, pp. 1121–1124.
  - [16] L. Duan, D. Zhang, F. Xu, and G. Cui, "A novel video encryption method based on faster r-cnn," in *2018 International Conference on Computer Science, Electronics and Communication Engineering (CSECE 2018)*. Atlantis Press, 2018, pp. 100–104.
  - [17] F. Almasalha, R. Hasimoto-Beltran, and A. A. Khokhar, "Partial encryption of entropy-coded video compression using coupled chaotic maps," *Entropy*, vol. 16, no. 10, pp. 5575–5600, 2014.
  - [18] J. I. M. Bezerra, G. Machado, A. Molter, R. I. Soares, and V. Camargo, "A novel simultaneous permutation–diffusion image encryption scheme based on a discrete space map," *Chaos, Solitons & Fractals*, vol. 168, p. 113160, 2023.
  - [19] Wikipedia contributors, "Poincaré recurrence theorem — Wikipedia, the free encyclopedia," 2023, [Online; accessed 8-March-2024].
  - [20] L. Xu and J. Zhang, "A novel four - wing chaotic system with multiple attractors based on hyperbolic sine: Application to image encryption\*," *Integration*, vol. 87, pp. 313–331, 2022.
  - [21] S. De, J. Bhaumik, and D. Giri, "A secure image encryption scheme based on three different chaotic maps," *Multimedia Tools and Applications*, vol. 81, no. 4, pp. 5485–5514, 2022.
  - [22] B. Rezaei, M. Mobasseri, and R. Enayatifar, "A secure, efficient and super-fast chaos-based image encryption algorithm for real-time applications," *Journal of Real-Time Image Processing*, vol. 20, no. 2, p. 30, 2023.
  - [23] Y. Bentoutou, E.-H. Bensikaddour, N. Taleb, and N. Bounoua, "An improved image encryption algorithm for satellite applications," *Advances in Space Research*, vol. 66, no. 1, pp. 176–192, 2020.
  - [24] A. Hafsa, M. Fradi, A. Sghaier, J. Malek, and M. Machhout, "Real-time video security system using chaos-improved advanced encryption standard (iaes)," *Multimedia Tools and Applications*, pp. 1–24, 2022.
  - [25] A. Carlson, G. Gang, T. Gang, B. Ghosh, and I. K. Dutta, "Evaluating true cryptographic key space size," in *2021 IEEE 12th Annual Ubiquitous Computing, Electronics & Mobile Communication Conference (UEMCON)*. IEEE, 2021, pp. 0243–0249.
  - [26] Y. Qobbi, A. Abid, M. Jarjar, S. E. Kaddouhi, A. Jarjar, and A. Benazzi, "Adaptation of a genetic operator and a dynamic s-box for chaotic encryption of medical and color images," *Scientific African*, vol. 19, p. e01551, 2023.
  - [27] D. S. Malik and T. Shah, "Color multiple image encryption scheme based on 3d-chaotic maps," *Mathematics and Computers in Simulation*, vol. 178, pp. 646–666, 2020.
  - [28] X. Liu, J. Mou, Y. Zhang, and Y. Cao, "A new hyperchaotic map based on discrete memristor and meminductor: Dynamics analysis, encryption application, and dsp implementation," *IEEE Transactions on Industrial Electronics*, vol. 71, no. 5, pp. 5094–5104, 2024.
  - [29] M. B. Farah, A. Farah, and T. Farah, "An image encryption scheme based on a new hybrid chaotic map and optimized substitution box," *Nonlinear Dynamics*, vol. 99, no. 4, pp. 3041–3064, 2020.
  - [30] J. Ferdush, M. Begum, and M. S. Uddin, "Chaotic lightweight cryptosystem for image encryption," *Advances in Multimedia*, vol. 2021, pp. 1–16, 2021.
  - [31] X. Hu, L. Wei, W. Chen, Q. Chen, and Y. Guo, "Color image encryption algorithm based on dynamic chaos and matrix convolution," *IEEE Access*, vol. 8, pp. 12 452–12 466, 2020.
  - [32] N. Mao, X. Tong, M. Zhang, and Z. Wang, "Real-time image encryption algorithm based on combined chaotic map and optimized lifting wavelet transform," *Journal of Real-Time Image Processing*, vol. 20, no. 2, p. 35, 2023.
  - [33] M. Li, M. Wang, H. Fan, K. An, and G. Liu, "A novel plaintext-related chaotic image encryption scheme with no additional plaintext information," *Chaos, Solitons & Fractals*, vol. 158, p. 111989, 2022.
  - [34] Y. Su, X. Wang, and H. Gao, "Chaotic image encryption algorithm based on bit-level feedback adjustment," *Information Sciences*, vol. 679, p. 121088, 2024.
  - [35] T. Umar, M. Nadeem, and F. Anwer, "Chaos based image encryption scheme to secure sensitive multimedia content in cloud storage," *Expert Systems with Applications*, vol. 257, p. 125050, 2024.
  - [36] M. Yildirim, "A color image encryption scheme reducing the correlations between r, g, b components," *Optik*, vol. 237, p. 166728, 2021.
  - [37] Q. Sheng, C. Fu, Z. Lin, M. Tie, J. Chen, and C.-W. Sham, "A one-time-pad-like chaotic image encryption scheme using data steganography," *Journal of Information Security and Applications*, vol. 78, p. 103592, 2023.
  - [38] S. Wang, Q. Peng, and B. Du, "Chaotic color image encryption based on 4d chaotic maps and dna sequence," *Optics & Laser Technology*, vol. 148, p. 107753, 2022.
  - [39] B. Jasra and A. Hassan Moon, "Color image encryption and authentication using dynamic dna encoding and hyper chaotic system," *Expert Systems with Applications*, vol. 206, p. 117861, 2022.
  - [40] B. Ge, X. Chen, G. Chen, and Z. Shen, "Secure and fast image encryption algorithm using hyper-chaos-based key generator and vector operation," *IEEE Access*, vol. 9, pp. 137 635–137 654, 2021.
  - [41] S. Tariq, M. Khan, A. Alghafis, and M. Amin, "A novel hybrid encryption scheme based on chaotic lorenz system and logarithmic key generation," *Multimedia Tools and Applications*, vol. 79, pp. 23 507–23 529, 2020.
  - [42] M. Gafsi, N. Abbassi, M. A. Hajjaji, J. Malek, and A. Mtibaa, "Improved chaos-based cryptosystem for medical image encryption and decryption," *Scientific Programming*, vol. 2020, pp. 1–22, 2020.